IJHSR
ijhighschoolresearch.org
RESEARCH ARTICLE

An Iterative Approach to Reconstruct the Phase of a Field from an X-Ray Free Electron Laser Intensity Measurement

Kenneth Shui

Monta Vista High School, 21840 McClellan Rd, Cupertino, CA 95014, USA; kshui2020@gmail.com
Mentor: Dr. Juhao Wu

ABSTRACT: In X-ray crystallography and Coherent Diffraction Imaging, only the diffraction patterns' light density can be directly measured, not its phase. The process of retrieving the phase is defined as the phase retrieval problem. In this project, I explore a classic iterative approach for phase retrieval to apply to an XFEL simulator real space data. The conventional Gerchberg-Saxton algorithm is modified and simulated. Two figures of merit are developed to quantify the algorithm's performance. Convergence time, initial phase, and noise sensitivity are evaluated. It is determined that the algorithm can be used to solve the phase problem for XFEL applications.

KEYWORDS: Physics and Astronomy; Atomic, Molecular, and Optical Physics; X-ray Free Electron Laser; Iterative Phase Retrieval; Strehl Ratio.

Introduction

Since the 1950s, X-ray diffraction has been used to discover DNA structure and take pictures of microscopic objects. In the past decades, scientists have managed to image macromolecular structures with orders of magnitude in the nanometers with the help of synchrotron light sources. These third-generation synchrotron light sources have a diffraction limit in the X-ray spectrum. However, scientists have encountered a new issue: Determining the structure and dynamics of proteins with orders of magnitude in the angstroms. Answering these questions requires X-ray free electron lasers (XFELs), a fourth-generation synchrotron light source capable of resolving proteins within their natural time scale of a few femtoseconds.[1]

Scientists can currently measure the intensity of a two-dimensional diffraction pattern by pointing an XFEL beam at a protein or protein crystal. By rotating the crystal, multiple diffraction patterns can be obtained and pieced into a three-dimensional image of the protein's shape. A simple illustration of the XFEL is shown in Figure 1. XFELs feature a short wavelength necessary for atomic-level measurement, an ultra-short time scale of a few femtoseconds to detect movement, and a high brilliance to illuminate atomic particles, opening new opportunities to probe the dynamics of ultrafast processes and protein structure at the atomic level.[2]

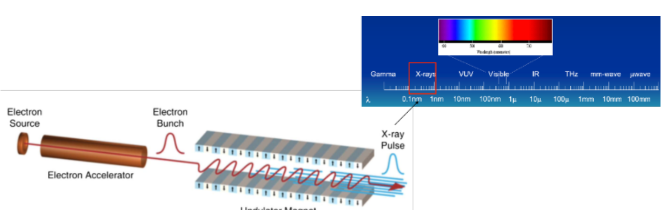

Figure 1: XFEL structure and the electromagnetic spectrum.

The coherent X-ray pulse produced by the XFEL in Figure 1 can then be used to perform coherent diffractive imaging (CDI), as shown in Figure 2.[3] An object is illuminated by a monochromatic coherent wave like an X-ray while the diffracted intensity is measured at the diffraction plane. This is also known as X-ray diffraction.

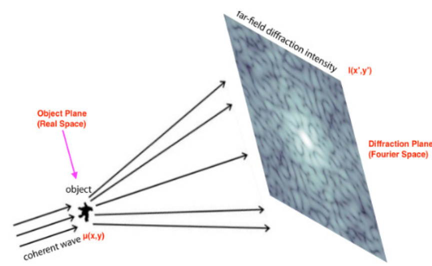

Figure 1: Coherent diffractive imaging (CDI) setup.

The diffraction space at position h is a complex quantity Uh, represented by magnitude |Uh| and phase Φh:

$$U_{\boldsymbol{h}} = |U_{\boldsymbol{h}}|e^{j\Phi_{\boldsymbol{h}}} \qquad \textit{Equation 1}$$

where h = {x',y',z'} is a 3D vector in Fourier space.

With the Fraunhofer approximation, also known as far-field approximation, the diffraction density I(x',y') is related to the 3D electron density of the object μ(x,y,z) through the Fourier Transform:

$$I(x',y') \propto |U_{\boldsymbol{h}}|^2 \propto \left|\iiint \mu(x,y,z)e^{j\frac{2\pi}{\lambda}\frac{-x'x-y'y}{z'}}dxdydz\right|^2 \qquad \textit{Equation 2}$$

If the Fourier phase is known, the electron density map and, thus, the 3D structure of the sample can be obtained through the inverse Fourier Transform as:

$$\rho(\boldsymbol{x}) = \frac{1}{V}\iiint U_{\boldsymbol{h}}e^{j\cdot 2\pi\cdot \boldsymbol{h}\cdot \boldsymbol{x}}d\boldsymbol{h} \qquad \textit{Equation 3}$$

where V is the volume of the object cell and *x* = {x,y,z} is a 3D vector in real space.

DOI: 10.36838/v5i5.11

One of the main challenges CDI and XFEL encounter is retrieving the phase, as the phase of the diffraction patterns cannot be directly measured easily. If the phase is known, scientists can determine the electron density of the protein through a Fourier synthesis, equivalent to determining the protein structure.[1] The process of retrieving the phase Φ_h is defined as the phase retrieval problem.

It is well known that knowledge of the Fourier phase is crucial in recovering an object from its Fourier transform.[4] Often, the Fourier phase contains more important information than its magnitude. An experiment to illustrate this is conducted in Figure 3. Two images (an astronaut and a soldier) are Fourier transformed. Their Fourier phases are swapped before being inversely Fourier transformed back into the image plane. It is clear that the Fourier phase contains a significant amount of information about these images. The observation holds true in coherent diffractive imaging and similar applications.

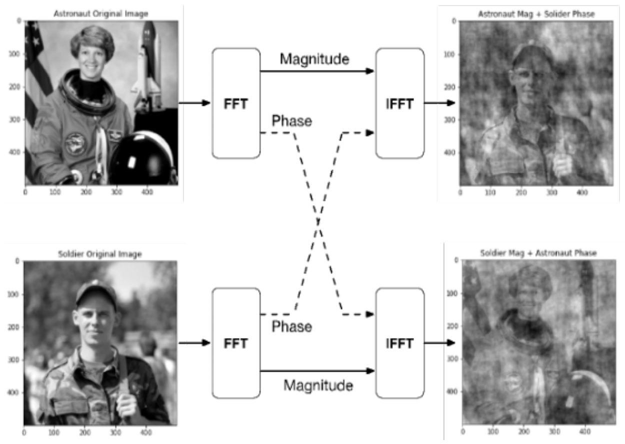

Figure 3: The importance of the Fourier phase.

To retrieve the phase, numerous phase retrieval techniques have been developed over the past decades, including direct methods,[5] iterative methods,[6,7] and, more recently, deep learning methods.[8]

The Gerchberg-Saxton (GS) algorithm is one of the popular iterative methods used for phase retrieval in many applications over decades. It can be categorized as one of the alternating projection methods. The GS algorithm only sometimes guarantees full convergence, as it can stagnate near the closest local minimum.[9] This limitation can be partially attributed to the non-convexity of the Fourier magnitude constraint.[10,11] Recently, progress has been made in giving theoretical convergence certificates.[12,13]

In this paper, we intend to investigate the effectiveness of a classic iterative phase retrieval algorithm for XFEL applications. We also wish to examine whether measurement errors like apparatus noise would affect the algorithm's effectiveness and to what extent. Finally, two objective figures of merit are proposed to evaluate the GS algorithm's performance.

Methods

The commonly used Gerchberg-Saxton (GS) phase retrieval algorithm is depicted in Figure 4.[6] It is one of the numerous phase retrieval techniques developed over the past decades.

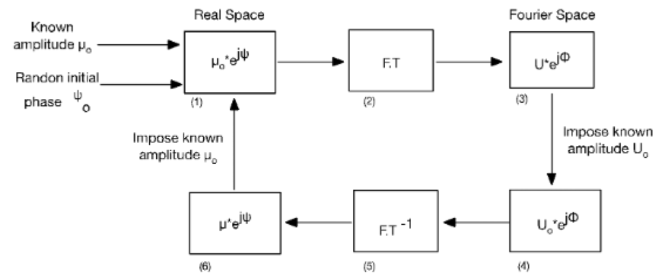

Figure 4: The Gerchberg-Saxton (GS) algorithm procedure.

The GS algorithm aims to retrieve phase from two intensity measurements: $|\mu_O|^2$ is the intensity from real space, and $|U_O|^2$ is the intensity from Fourier space. The algorithm uses the following steps to recover the complex-valued distributions $\mu e j^{\Psi}$ in real space and $U e j^{\Phi}$ in Fourier space:

(1) Create an initial complex input by combining the measured amplitude μ_O with a random phase ψ_O.

(2) Perform a Fourier transform on the complex input into Fourier space.

(3) Obtain a complex pair of amplitude U and phase Φ.

(4) Impose a Fourier space amplitude measurement Uo onto the transformed output $U e j^{\Phi}$ in step (3), creating an updated Fourier space distribution $U e j^{\Phi}$.

(5) Perform an inverse Fourier transform back into real space and get the complex value $\mu e j^{\Psi}$.

(6) Impose a real space amplitude measurement μ_O onto $\mu e j^{\Psi}$ in step (5), creating an updated real space distribution $\mu_O e j\psi$ as an updated amplitude for the next iteration starting again at step (1).

Only real space (time-domain) XFEL field data is available in our research. Unfortunately, we don't have the Fourier space (frequency-domain) intensity data from the XFEL simulator. Therefore, we modified the traditional GS algorithm accordingly, as shown in Figure 5 below.

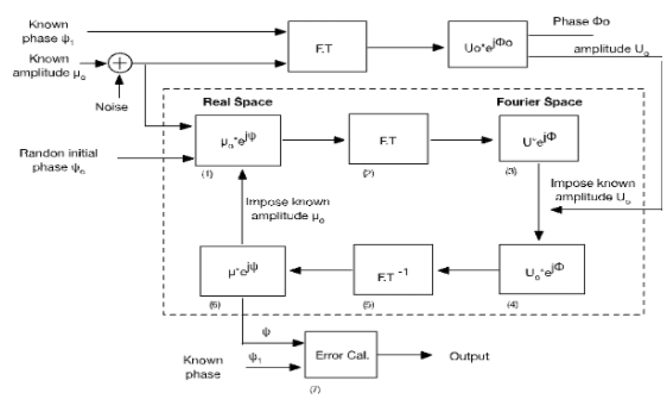

Figure 5: Modified GS algorithm procedure.

The main difference stems from step (4): The Fourier transform of the known input $\mu o e j^{\Psi}$ is obtained as $U o e j^{\Phi}$ to serve as the Fourier space measurement instead of the measured/simulated Fourier space amplitude. Uo is used to replace U in step (4) to continue the iteration process.

The performance of the modified GS algorithm in the XFEL application is carried out in step (7) of Figure 5. To

DOI: 10.36838/v5i5.11

check the noise immunity and robustness of the algorithm, noise is injected at the real space known input shown in Figure 5. More details of the noise experiment will be discussed in Section **Results and Discussion**.

Although we conduct phase retrieval in real space (time domain), the Fourier space phase is retrieved simultaneously through our experiment. Therefore, time domain phase retrieval and frequency domain phase retrieval are equivalent.

Introduction

Data Source:

The research's input data comes from an XFEL emulator's output, as shown in Figure 6(a). Complex values of an electric field are obtained in a 2-D plane and distributed across the coordinates (xgrid, ygrid), xgrid ∈ [0, 300], ygrid ∈ [0, 300], at a given time, as shown in Figure 6(b). Each grid unit represents 1.33μm by 1.33μm in real physical space. The field is measured at a different time interval or the so-called n-slice number. The E-field complex data in the form of a magnitude and phase pair is used as input to our research setup shown on the left side of Figure 5.

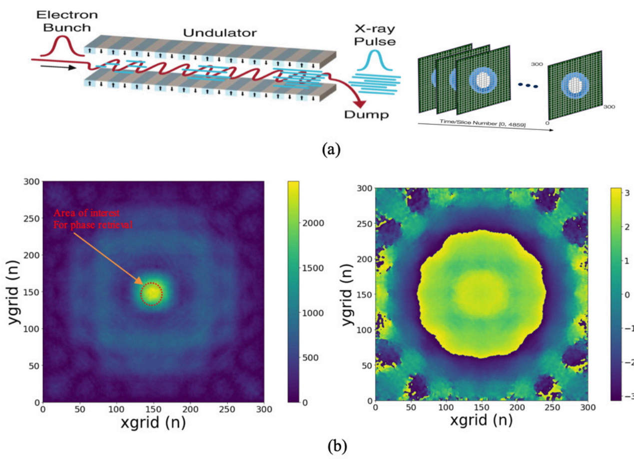

Figure 6: Experiment setup (a) and electric field (b): magnitude (left) and phase (right).

Phase Retrieval with Gaussian Beam and FEL:

XFELs can be modeled as a sum of the Gaussian Beam base function in time:[2]

$$E(t) = \sum_k A_k \cdot e^{i(\omega_k \cdot t+\varphi_k)-\frac{(t-t_k)^2}{2\cdot\sigma_{kt}^2}} \qquad \text{Equation 4}$$

As the first step, the modified GS algorithm is used to check the Gaussian Beam (k=1) and multimodal XFEL (k=4), whose results are shown in the upper and lower halves of Figure 7, respectively. The left half represents the ground-truth input unwrapped phase (red), retrieved unwrapped phase (blue) and initial random wrapped phase (green) of the Gaussian Beam signal, while the right half represents the magnitude of ground-truth (red) and retrieved (blue) Gaussian Beam. For the k=1 case, the retrieved phase (red) completely matches the input phase (blue). For the k=4 case, the retrieved phase also matches the ground-truth input phase quite well. In Figures 7-16, any instance of "phase" refers to "unwrapped phase."

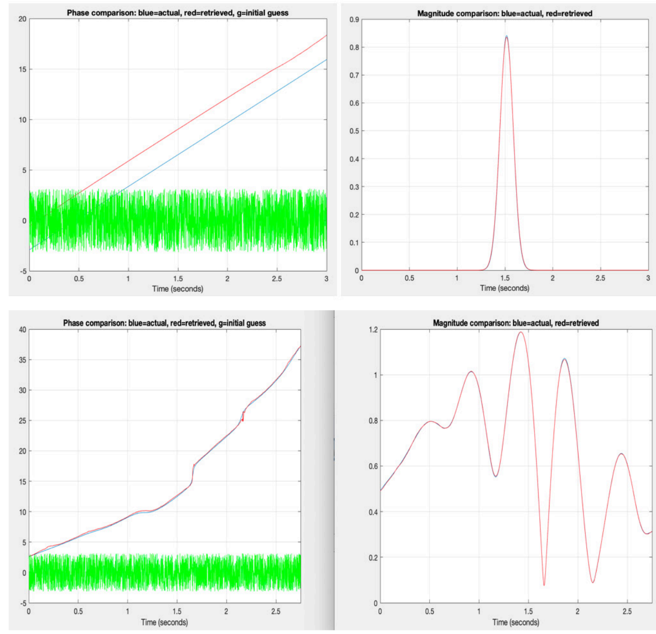

Figure 7: GS algorithm to retrieve single-mode (top) and multimodal XFEL (bottom).

Single Electric Field Simulation Result:

Secondly, data from an XFEL emulator is used. An electric field with n-grid = (150, 150) is applied as input, and a random initial phase is used inside the GS program. One of the simulated outputs is shown in Figure 8 below, with the

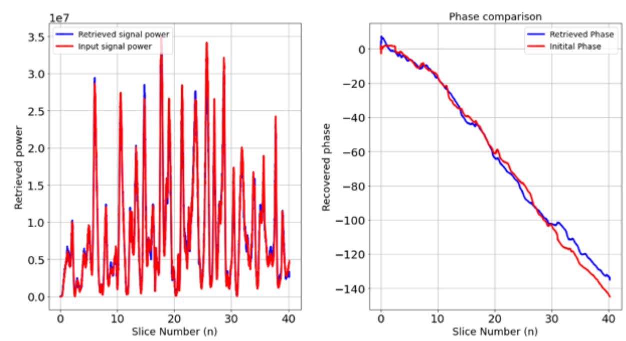

Figure 8: Retrieved magnitude (left) and unwrapped phase (right) of a single field.

retrieved amplitude and unwrapped phase shown on the left and right, respectively.

Multiple Electric Field Simulation Comparison:

Next, we choose a few combinations of electric field sets and check the phase retrieval effectiveness. The simulation result is shown in Figure 9 below. Again, the left column plots show the phase comparison while the right column plots show the corresponding E-field power.

We see that as the n-grid varies among (100, 100), (150, 150), (200, 200), and (250, 250), the transverse fields have multiple modes, which leads to significant variation in the ground truths of their phases. The retrieved phase error will thus vary depending on the E-field coordinates. The E-field power is most potent at (150, 150), which indicates a sinretrieval is expected to work best when a strong, single-mode transverse electromagnetic (TEM) mode exists. As a result, our following phase retrieval experiment will focus on the (150, 150) grid field.

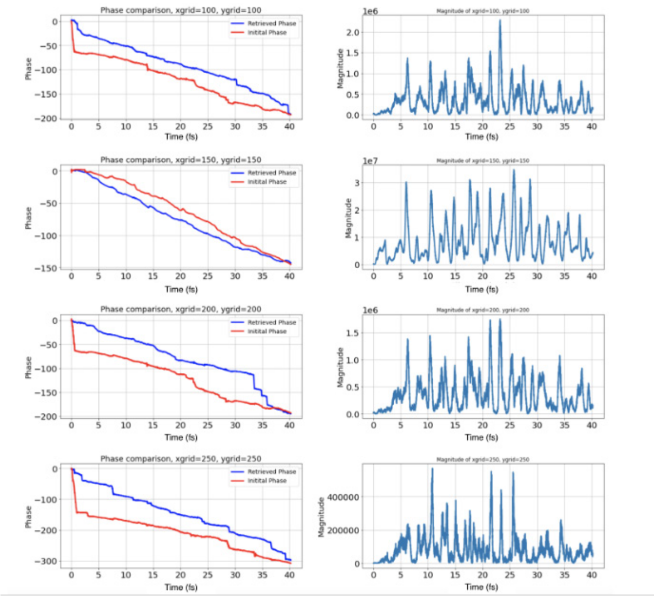

Figure 9: Comparison of different E-field phase retrieval and power.

The performance of the phase retrieval algorithm for multimodal fields can be better gauged with the Strehl Ratio metric described in Section **Phase Retrieval Performance Evaluation Using Strehl Ratio (SR)**.

Phase Retrieval Performance Evaluation Using First-Order Norm:

To find out the performance of the GS-based phase retrieval on this XFEL application, we take the normalized first-order error (F_error) between the known phase (φ_k) and retrieved phase ($\widehat{\varphi_k}$) as the figure of merit:

$$F\_error = \frac{\sum_{k=1}^{N} |\varphi_k - \widehat{\varphi_k}|}{\sum_{k=1}^{N} |\varphi_k|} \qquad \textit{Equation 5}$$

We perform the following procedure:

1. Determine the F_error of the input EM fields with respect to each other in the vicinity of the (150, 150) grid. A total of five n-grid coordinates are examined: (149, 150), (150, 149), (150, 150), (150, 151), and (151, 150). This step reveals the phase 'resolution' of the known E-field.
2. Determine the F_error of the retrieved phase vs. ground-truth input phase for all five coordinates in the vicinity of (150, 150).
3. Compare the results of step 2 with step 1.

Suppose the F_error of step 2 is smaller or equivalent to that of step 1. In that case, we declare that our current GS-based algorithm achieves the desired accuracy since the error introduced through phase retrieval is comparable to the phase 'resolution' of the input E-field. In other words, our error is smaller than our unit of measure.

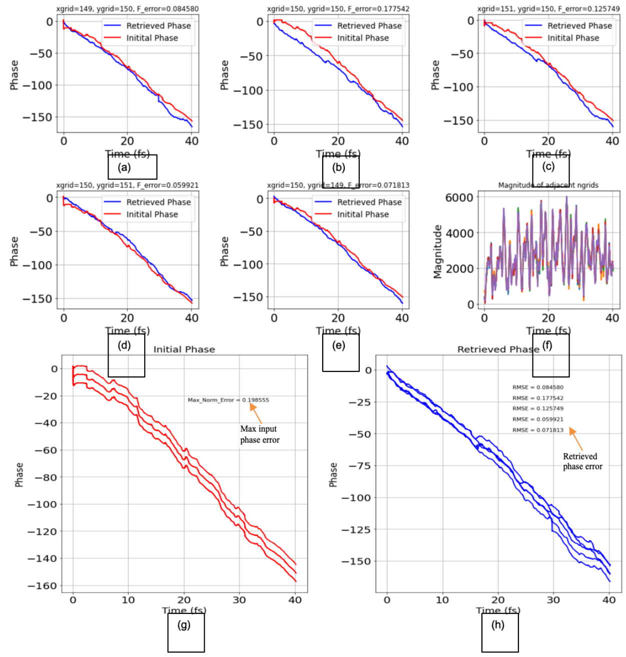

Figure 10: Phase retrieval error check across adjacent fields.

The retrieved phase and ground-truth known input phase of the five adjacent grid coordinates are shown in Figure 10(a, b, c, d, e). Their power/magnitude is also shown in the small lower right corner plot, Figure 10(f), to ensure that these fields closely resemble a single-mode TEM field. The maximum input phase error measured between two adjacent n-grid areas is shown on the large left plot, Figure 10(g). The retrieved phase error, defined as the error between the ground-truth phase and the retrieved phase for each of the five cases, is shown on the large right plot, Figure 10(h).

The algorithm converges quite well in our simulation studies, usually converging in less than 1500 iterations, with a random phase assigned in the first step of Figure 5. The convergence criteria are defined as when the retrieved phase is equivalent to or smaller than the error budget described above. For example, one convergence iteration for an n-grid = (150, 150) simulation is shown in Figure 11.

Our simulation indicates that the retrieved phase error is smaller than the phase error at the input neighborhood region. Therefore, we conclude that our GS-based phase retrieval achieves satisfactory accuracy using the figure of merit defined in this section.

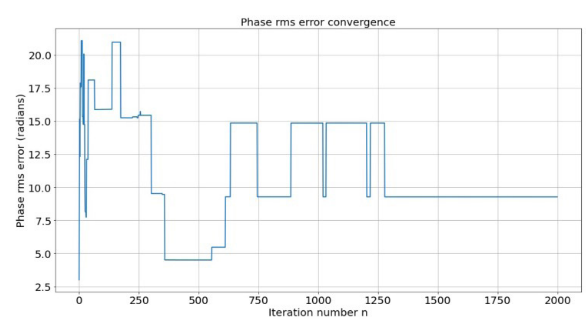

Figure 11: Retrieved phase convergence with iteration runs.

DOI: 10.36838/v5i5.11

Phase Retrieval Performance with Additive Noise :

In our setup, we inject Gaussian random noise at the time domain signal magnitude, as shown in Figure 5, if we assume that the measurement apparatus has built-in hardware limitations. The following equation determines the standard deviation of the noise σ_n:

$$\sigma_n = \sqrt{\frac{\sigma_s^2}{SNR}} \qquad \text{Equation 6}$$

where SNR is the signal power to noise power ratio, and σ_s is the signal standard deviation derived from the time domain magnitude calculation at n-grid (150, 150). It should be noted that when the input signal amplitude is corrupted, we assume that its Fourier domain constraint counterpart will also be affected, as shown in Figure 5.

The phase retrieval performance is then compared between a clean input signal without noise and a corrupted input signal with a certain SNR. The results are shown in Figure 12, where the retrieved phase F_error measured between two adjacent n-grid areas is compared. A slight increase of F_error of the right plot (corrupted case) against the center plot (clean signal case) is observed.

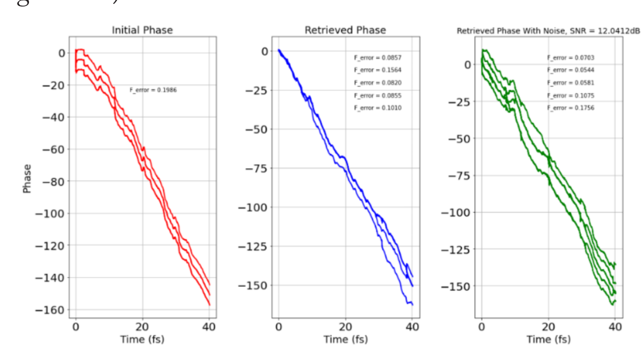

Figure 12: GS phase retrieval noise sensitivity via F_error comparison.

Figure 13 shows the plot where the phase retrieval F_error is swept with a different SNR with two choices of n-grids. The following observations can be made:

Poor SNR significantly impacts the GS-based algorithm's accuracy compared with the ideal case. For example, we see a five-fold increase of F_error when SNR < 1.

There is a certain dependency on the choice of the n-grid coordinates. For example, the (149, 150) ideal case has a lower initial F_error than the (150, 150) case. It also converges faster than the (150,150) case.

When SNR is sufficiently high (SNR > 10), the impact of additive noise on the retrieved phase accuracy is negligible as the two curves start to converge.

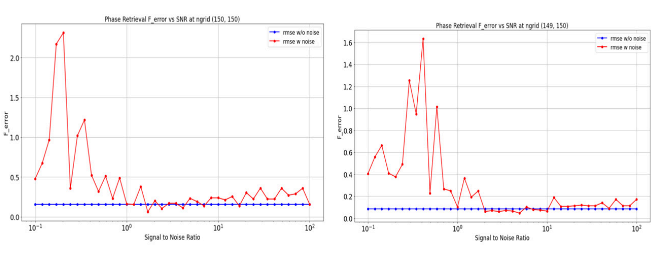

Figure 13: GS phase retrieval noise sensitivity via F_error comparison.

Phase Retrieval Performance Evaluation Using Strehl Ratio (SR):

The Strehl ratio (SR) is a parameter frequently used in optics. It is defined as the ratio of the highest density in the aberrated image from a point source to the maximum intensity achievable from a perfect aperture limited by diffraction.[14,15] It can usually be estimated using only the statistics of the phase deviation Φ:

$$S = e^{-\sigma^2} \qquad \text{Equation 7}$$

where σ is the root mean square phase deviation over the aperture of the wavefront, and S is a value ranging from 0.0 to 1.0. When there is no phase error, S becomes 1.0. Thus, we can use the Strehl ratio to evaluate phase retrieval performance as a more objective figure of merit.

In our experiment, the Strehl ratio can be used to check whether a single-mode or multi-mode E-field exists in a given grid area, as shown in Figure 14 below. In Figure 14(a), the full area (0, 300) is included, and the Strehl ratio is relatively low and has little dependency over light intensity. This indicates that multiple modes exist across the vast region of (0, 300). In Figure 14(b), the area is constrained to (130, 170), and the Strehl ratio approaches 1.0 in many slices, suggesting a strong positive correlation between intensity and Strehl ratio. This indicates that most of the time, or for most slices, a single-mode E-field exists in the reduced area (130, 170).

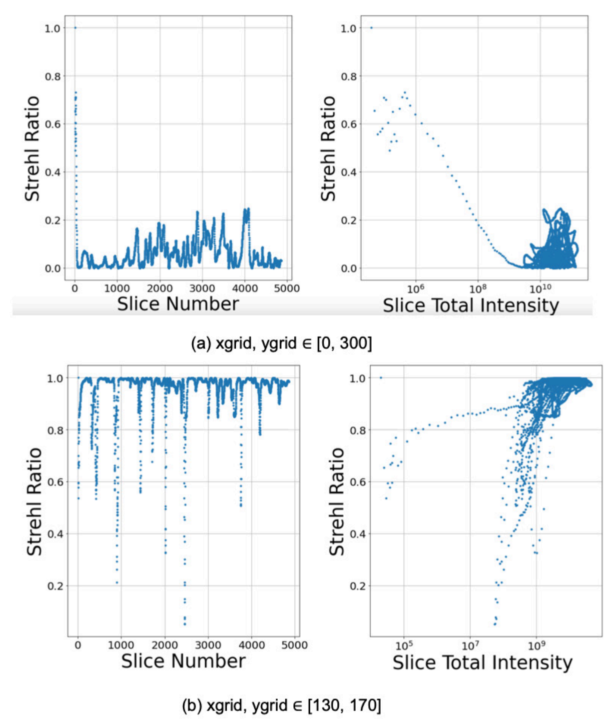

Figure 14: Strehl ratio for unimodal and multimodal E-field regions.

As previously explained in **Section Single Electric Field Simulation Result**, our modified GS algorithm works well in the center region (150, 150) where a single mode E-field dominates. This is confirmed by examining the Strehl ratio across different regions, as shown in Figure 15.

Inspecting Figure 15(a), we see that the Strehl ratio of the retrieved field (red) is, on average, much lower than that of the original field (blue) across the slice/time. This is attributed to the existence of a multimodal E-field in the grid region (100, 200). We can also verify this by inspecting Figure 15(b). When the grid region is more centralized within (145, 155) where a single mode exists, the Strehl ratio of the retrieved field (red) tracks the original field (blue) much better. This illustrates again that our modified GS algorithm works quite well for single-mode E-field regions.

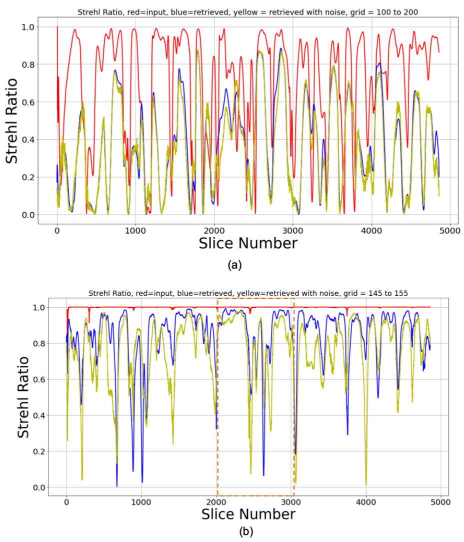

Figure 15: Comparing Strehl Ratios at different regions.

The noise impact on the phase retrieval is also examined using the Strehl ratio parameter. With SNR=10, we see that there are noticeable degradations for the retrieved phase accuracy by comparing the yellow curve with the blue curve in Figure 15(b).

One may question that even with a single mode E-field situation like that in Figure 15(b), there are times when the Strehl ratio of the retrieved field is still much lower than the original field (ground truth), such as when the slice ranges from 2000 to 3000.

As shown in Figure 16, a comparison is made between the Strehl ratio (upper plot) and field intensity (lower plot). Clearly, there is a strong positive correlation between the Strehl ratio and field intensity. When the field intensity is low (below 107), our GS-based algorithm cannot produce accurate phases to yield high Strehl ratios, like when the slice number is 2000, 2700, or 3000. On the other hand, when the field intensity is high, our GS-based algorithm can retrieve phases quite well to yield high Strehl ratios, like when the slice number is 2100, 2300, or 2900.

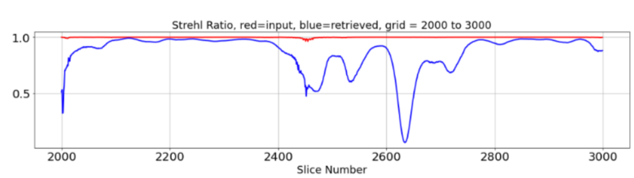

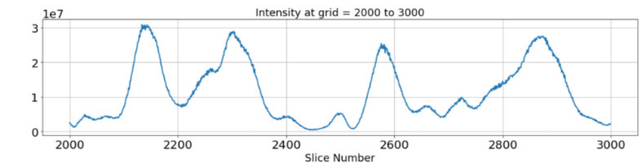

Figure 16: Single-mode E-Field Strehl Ratio vs. field intensity.

Conclusion

In conclusion, both children and adults with AATD have anThe modified GS algorithm is employed in the XFEL E-field phase retrieval application. By imposing a time-domain magnitude constraint and a Fourier-transformed frequency domain magnitude constraint, the phase of the E-field at the time domain can be successfully retrieved with acceptable error tolerance. This research also introduces measurement apparatus-induced error to determine the modified GS algorithm's robustness under non-ideality. We find that with a reasonable signal-to-noise ratio (SNR > 3 in some cases), the additive noise-induced error is still within the acceptable error budget of the system.

Two objective figures of merit are used to evaluate the performance of the modified GS algorithm: the First-order normalized error (F_error) and the Strehl ratio. In addition, the cause of a large phase error is analyzed and verified. We conclude that the proposed GS phase retrieval algorithm can achieve remarkable accuracy when a single mode E-field with sufficient intensity power is available for the XFEL application.

Acknowledgments

I express my sincere gratitude to my research mentor Dr. Juhao Wu. Throughout the months of research, I learned so much from him, whether it be about X-ray crystallography, data convexity, or signal processing. I cannot imagine having a better mentor for my research studies. His knowledge, guidance, and unwavering support have made this work possible. Furthermore, his positive attitude inspires me to develop an enthusiastic passion for physics research.

References

1. Neutze, R., Brändén, G., & Schertler, G. F. X. "Membrane Protein Structural Biology Using X-Ray Free Electron Lasers." Current O pinion in Structural Biology, Elsevier Current Trends, 3 Sept. 201 5.
2. Emma, P., Akre, R., & Arthur, J. SLAC, Stanford University, " Intr oduction to the Physics of Free-Electron Lasers," https://web.stanford.edu/group/pulse_institute/static/uxss2016/UX SS2016-Mar inelli(1).pdf.
3. Shechtman, Y., Eldar, Y. C., Cohen, O., Chapman, H. N., Miao, J., & Segev, M. "Phase retrieval with application to optical imaging," IEEE Signal Processing Magazine, vol. 32, issue 3, pp. 87 - 109, 2 015.
4. Oppenheim, A. V., & Lim, J. S. "The importance of phase in signal s," Proceedings of the IEEE, vol. 69, no. 5, pp. 529-541, 1981.
5. Iacnois, C. "Spectral phase interferometry for direct electric-field r econstruction of ultrashort optical pulses," Optical Letters, vol. 23, No. 10, May 5, 1998.
6. Gerchberg, R. W., & Saxton, W. O. "A practical algorithm for the determination of phase from image and diffraction plane pictures, " Optik 35, 237-246 (1972).

DOI: 10.36838/v5i5.11

7. Fienup, J. R. "Reconstruction of an object from the modulus of its Fourier Transform," Optical Letters 3, 27-9, 1978.
8. Nishizaki, Y., Horisaki, R., Kitaguchi, K., Saito, M., & Tanida, J. "Analysis of non-iterative phase retrieval based on machine learni ng," Optical Review (2020) 27:136-141.
9. Fannjiang, A., & Liao, W. "Phase retrieval with random phase illu mination," J. Opt. Soc. Am. A 29, 1847-1859, 2012.
10. Levi, A., & Stark, H. "Image restoration by the methods of gene ralized projections with application to restoration from magnitude ," J. Opt. Soc. Am. A 1, 932-943, 1984.
11. Bauschke, H. H., Combettes, P. L., & Luke, D. R. "Phase retrievel , error reduction algorithm, and Fienup variants: a view from conv ex optimization," J. Opt. Soc. Am. A 19, 1334-1345, 2002.
12. Noll, D. "Alternating projections with applications to Gerchberg -Saxton Error Reduction," https://doi.org/10.1007/ s11228-021-00585-1, July 2021.
13. Noll, D., & Rondepierre, A. "On local convergence of the metho d of alternating projections," The Journal of the Society for the Fo undations of Computational Mathematics, 16: 425-455, 2016.
14. Sacek, V. "6.5. Strehl ratio" (https://www.telescope-optics.net/Str ehl.htm), Notes on amateur telescope optics, March 2, 2011.
15. Mahajan, V. "Strehl ratio for primary aberrations in terms of their aberration variance," J. Opt. Soc. Am., 73 (6): 860-861, 1983.

Author

Kenneth Shui is a senior at Monta Vista High School. He has a strong passion for mathematics and physics and interests in humanities and volunteering. Hobbies like singing and volleyball further enrich his life. He hopes to continue particle physics research in college.